Surface and interfacial dynamics of polymeric bilayer films

Zhang Jiang,[1] Hyunjung Kim,[2,*] Simon G. J. Mochrie,[3] L. B. Lurio,[4] and Sunil K. Sinha[1,5]
[1]*Department of Physics, University of California at San Diego, La Jolla, California 92093, USA*
[2]*Department of Physics and Interdisciplinary Program of Integrated Biotechnology, Sogang University, Seoul 121-742, Korea*
[3]*Departments of Physics and Applied Physics, Yale University, New Haven, Connecticut 06520, USA*
[4]*Department of Physics, Northern Illinois University, DeKalb, Illinois 60115, USA*
[5]*LANSCE, Los Alamos National Laboratory, Los Alamos, New Mexico, 87545, USA*
(Received 15 February 2006; published 19 July 2006)

The theory for surface dynamics of the thermally excited fluctuations on a homogenous single-layer film of arbitrary depth is generalized to describe surface and interfacial dynamics of polymeric liquid bilayer films in terms of susceptibilities, power spectra, and characteristic relaxation time constants. The effects on surface dynamics originating from viscosity inhomogeneities close to the surface and interfacial regions are investigated by the bilayer theory and compared with the surface dynamics of homogeneous single-layer films under nonslip and slip boundary conditions. Our bilayer theory can also be extended to study interfacial dynamics of more generalized multilayer systems. The effects of viscoelasticity and van der Waals interactions on surface and interfacial dynamics are also briefly discussed.

DOI: 10.1103/PhysRevE.74.011603 PACS number(s): 68.15.+e, 82.35.Gh, 61.10.Eq, 68.03.Kn

I. INTRODUCTION

It is well known that liquid surfaces are decorated by thermally excited capillary waves, and extensive theoretical and experimental studies have been performed to determine the static surface structures. With regard to dynamic properties of these thermal fluctuations, the complete spectra and dynamics of the capillary waves on homogeneous bulk liquids and supported liquid single-layer films have been studied theoretically [1,2]. Using the classical fluctuation dissipation theorem, the spectrum of small-amplitude thermal capillary waves can be derived from the dynamic susceptibility $\chi_{zz}(k,\omega)$, which specifies the linear response of the surface height to a periodic external force field acting vertically on the liquid surface. Capillary waves are expected to damp and propagate along the surface. However, on highly viscous liquids, such as polymeric melts, the damping is so large that all modes become over-damped. The spectrum of these over-damped capillary waves with a particular wavelength takes a Lorentzian shape centered at zero frequency with the width being the characteristic relaxation rate. Recently a technique, x-ray photon correlation spectroscopy (XPCS) [3–6], has been developed to examine these surface waves on a much smaller lateral length scale than can be achieved with traditional dynamic light scattering (DLS) [7,8] and on a slower time scale than neutron spin echo technique can usually reach. For bilayer or even multilayer films, XPCS is the only technique to measure interfacial dynamics directly by tuning the x-ray incident angle to excite x-ray standing waves and selectively enhance the illumination and thus scattering at a particular interface [9,10].

It is very important to understand polymer surfaces and interfaces from the basic scientific point of view. There are still many issues far from being well understood, e.g., substrate-polymer interactions, the static conformations and the dynamical behaviors of polymer chains close to surfaces and interfaces. In particular, viscoelastic polymers show different behaviors from those in the bulk state when the length scale of the system gets smaller and smaller. Take the controversial glass transition as an example. The glass transition temperature T_g was found in certain studies to show a pronounced reduction for silicon supported thin polystyrene (PS) films [11–13]. It was proposed that near the free surface there exists a thin liquidlike layer with lower viscosity, i.e., polymer chains and/or segments have more mobility at the surface than in the bulk [14–16]. Moreover, the study of the surface and interfacial dynamics of bilayer films might shed light into deeper understandings of the mechanisms of interfacial lubrication and adhesion, coating stability, and so on. To properly investigate such phenomena using scattering methods, it is necessary to construct an appropriate theoretical expression for $\chi_{zz}(k,\omega)$. To this end, in Sec. II we present equations of motion and boundary conditions for a supported bilayer liquid film, from which the surface and interfacial susceptibilities, fluctuation power spectra (or intermediate scattering functions), roughnesses, and relaxation modes are derived. In Sec. III, the surface dynamics from single-layer films with different substrate boundary conditions are discussed, permitting investigation of the effects of the possible mobility inhomogeneity on single-layer film surface dynamics. In Sec. IV, we briefly discuss the surface and interfacial dynamics of linear viscoelastic liquids with frequency-dependent viscosities.

II. SURFACE AND INTERFACIAL DYNAMICS OF A SUPPORTED BILAYER FILM

Consider a liquid bilayer film on a solid substrate (Fig. 1) with bottom layer thickness h_1 and top layer thickness $h_2 = d - h_1$. For clarity, we use subscript and superscript 1 and 2

*Electronic address: hkim@sogang.ac.kr

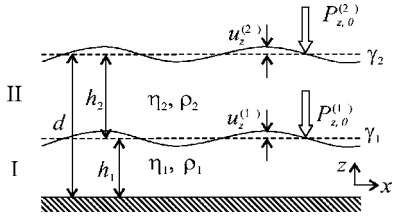

FIG. 1. Geometry and notations of a supported bilayer film. Bottom layer and top layer are denoted by region I and II, respectively.

to represent the parameters related to the bottom and top layers, and the interface and free surface, respectively. For example, the dynamic viscosity and the mass density of the top layer II are denoted by η_2 and ρ_2. The surface and interfacial tensions are γ_2 and γ_1, respectively. We assume small periodic externally applied pressure perturbations on the interface and the free surface of the form $P_{z,0}^{(1)}e^{i(kx-\omega t)}$ and $P_{z,0}^{(2)}e^{i(kx-\omega t)}$, respectively, with $u_z^{(1)}$ and $u_z^{(2)}$ being the vertical displacements of the reactive fluctuations. The media are supposed to be uniform throughout each layer so that the mass density profile is composed of step functions on which are superimposed surface and interfacial fluctuations with small amplitudes.

We start with the linearized Navier-Stokes equation for incompressible liquids [2]

$$\partial_t \boldsymbol{v} = -\frac{1}{\rho}\nabla p + \nu\nabla^2 \boldsymbol{v}, \tag{1}$$

where $\boldsymbol{v}$, and p are velocity field and pressure, and $\nu=\eta/\rho$ is the kinematic viscosity of the liquid. In the following calculations, a frequency-independent viscosity will be used. However, to take into account the elasticity effect of a viscoelastic liquid, one can explicitly substitute ν by a frequency-dependent kinematic viscosity, for example, a simple constitutive Maxwell-Debye model $\nu(\omega)\simeq\nu+i\mu/(\omega\rho)$, where μ represents the real and frequency-independent shear modulus. In Eq. (1) the gravitational potential is effectively treated as part of the pressure. We then try to look for solutions for the velocity and pressure in the form of monochromatic plane waves propagating along the x direction,

$$\boldsymbol{v}^{(j)}(\boldsymbol{r},t) = [V_x^{(j)}(z)\boldsymbol{e}_x + V_z^{(j)}(z)\boldsymbol{e}_z]e^{i(kx-\omega t)}, \tag{2a}$$

$$p^{(j)}(\boldsymbol{r},t) = P^{(j)}(z)e^{i(kx-\omega t)}, \tag{2b}$$

where the superscript $j=1,2$ denotes the solutions in region I and II, respectively.

A. Region I, II and boundary condition at $z=0$

Jäckle derived the velocity and pressure fields within a uniform single-layer film [2]. In a similar way for a bilayer film, applying the monochromatic plane-wave assumption, Eqs. (2), as well as the equation of continuity, $\nabla\cdot\boldsymbol{v}=0$, in terms of velocity amplitudes

$$ikV_x^{(j)} + \partial_z V_z^{(j)} = 0, \tag{3}$$

Eq. (1) leads to the preliminary solutions of the Navier-Stokes equation in region I and II:

$$V_z^{(j)}(z) = A_k^{(j)}\cosh(kz) + B_k^{(j)}\sinh(kz) + ik\hat{B}_j\cosh(\kappa_j z) + ik\hat{C}_j\sinh(\kappa_j z), \tag{4a}$$

$$V_x^{(j)}(z) = \frac{i}{k}\partial_z V_z^{(j)}(z), \tag{4b}$$

$$\frac{P^{(j)}(z)}{\rho_j} = \frac{i\nu_j}{k}(\kappa_j^2 - \partial_z^2)V_x^{(j)}(z), \tag{4c}$$

where $\kappa_j=\sqrt{k^2-i\omega/\nu_j}$, and $A_k^{(j)}$, $B_k^{(j)}$, $\hat{B}_j$, and $\hat{C}_j$ are constants to be determined by the boundary conditions at $z=0$, h_1, and d.

The nonslip boundary condition at $z=0$ reads $V_x^{(1)}|_{z=0} = V_z^{(1)}|_{z=0}=0$, yielding $A_k^{(1)}=-ik\hat{B}_1$ and $B_k^{(1)}=-i\kappa_1\hat{C}_1$. If the xz and zz components of the stress tensor in regions I and II are denoted as

$$\sigma_{xz}^{(j)} \equiv \hat{\sigma}_{xz}^{(j)}e^{i(kx-\omega t)} = \eta_j(\partial_z v_x^{(j)} + \partial_x v_z^{(j)}), \tag{5a}$$

$$\sigma_{zz}^{(j)} \equiv \hat{\sigma}_{zz}^{(j)}e^{i(kx-\omega t)} = -p^{(j)} + 2\eta_j\partial_z v_z^{(j)}, \tag{5b}$$

then Eqs. (4) and (5a) can be combined into compact matrix expressions:

$$\mathbf{X} = \mathbf{B}\mathbf{Z}, \quad \text{region I}, \tag{6a}$$

$$\mathbf{W} = \mathbf{A}\mathbf{Y}, \quad \text{region II}, \tag{6b}$$

where $\mathbf{X}$ and $\mathbf{Z}$, $\mathbf{W}$ and $\mathbf{Y}$ are defined for region I and II, respectively, as

$$\mathbf{X} = \begin{bmatrix} V_x^{(1)} \\ V_z^{(1)} \\ P^{(1)}/\rho_1 \\ \hat{\sigma}_{xz}^{(1)} \end{bmatrix}, \quad \mathbf{Z} = \begin{bmatrix} \hat{B}_1 \\ \hat{C}_1 \end{bmatrix}, \tag{7a}$$

$$\mathbf{W} = \begin{bmatrix} V_x^{(2)} \\ V_z^{(2)} \\ P^{(2)}/\rho_2 \\ \hat{\sigma}_{xz}^{(2)} \end{bmatrix}, \quad \mathbf{Y} = \begin{bmatrix} A_k^{(2)} \\ B_k^{(2)} \\ \hat{B}_2 \\ \hat{C}_2 \end{bmatrix}, \tag{7b}$$

and the matrices $\mathbf{B}$ and $\mathbf{A}$ are defined as

$$\mathbf{B} = \begin{bmatrix} k\sinh(kz) - \kappa_1 \sinh(\kappa_1 z) & \kappa_1 \cosh(kz) - \kappa_1 \cosh(\kappa_1 z) \\ -ik\cosh(kz) + ik\cosh(\kappa_1 z) & -i\kappa_1 \sinh(kz) + ik\sinh(\kappa_1 z) \\ \omega \sinh(kz) & \omega(\kappa_1/k)\cosh(kz) \\ 2\eta_1 k^2 \cosh(kz) - \eta_1(k^2+\kappa_1^2)\cosh(\kappa_1 z) & 2\eta_1 k\kappa_1 \sinh(kz) - \eta_1(k^2+\kappa_1^2)\sinh(\kappa_1 z) \end{bmatrix}, \tag{8a}$$

$$\mathbf{A} = \begin{bmatrix} i\sinh(kz) & i\cosh(kz) & -\kappa_2 \sinh(\kappa_2 z) & -\kappa_2 \cosh(\kappa_2 z) \\ \cosh(kz) & \sinh(kz) & ik\cosh(\kappa_2 z) & ik\sinh(\kappa_2 z) \\ (i\omega/k)\sinh(kz) & (i\omega/k)\cosh(kz) & 0 & 0 \\ 2ik\eta_2 \cosh(kz) & 2ik\eta_2 \sinh(kz) & -\eta_2(k^2+\kappa_2^2)\cosh(\kappa_2 z) & -\eta_2(k^2+\kappa_2^2)\sinh(\kappa_2 z) \end{bmatrix}. \tag{8b}$$

Hence, the hydrodynamic problem reduces to the problem of solving for coefficients $\mathbf{Y}$ and $\mathbf{Z}$ via the other two boundary conditions at $z=h_1$ and d.

B. Interfacial boundary condition at $z=h_1$

If the bilayer system is composed of two immiscible liquids, the interfacial boundary condition in equilibrium is that the velocities of the liquids on both sides at the interface must be equal and that the forces that each exerts on the other must be equal and opposite:

$$V_x^{(2)} = V_x^{(1)}, \quad V_z^{(2)} = V_z^{(1)}, \tag{9a}$$

$$\hat{\sigma}_{xz}^{(2)} = \hat{\sigma}_{xz}^{(1)}, \tag{9b}$$

$$\hat{\sigma}_{zz}^{(2)} - \hat{\sigma}_{zz}^{(1)} = [\gamma_1 k^2 + g(\rho_1 - \rho_2)]U_z^{(1)} - P_{z,0}^{(1)}, \tag{9c}$$

where $U_z^{(1)}$ is the amplitude of the vertical displacement of interfacial fluctuations evaluated by $u_z^{(1)} = \frac{i}{\omega} v_z^{(1)}|_{z=h_1}$. Here in writing the boundary condition Eq. (9c), the gravitational potential has to be included explicitly. Again with the equation of continuity Eq. (3) in both layers, one can rewrite the interfacial boundary condition in a matrix form

$$\mathbf{W}|_{z=h_1} = \mathbf{TX}|_{z=h_1} + \mathbf{U}, \tag{10}$$

where $\mathbf{U}$ and $\mathbf{T}$ are defined as follows:

$$\mathbf{U} = \begin{bmatrix} 0 & 0 & \frac{P_{z,0}^{(1)}}{\rho_2} & 0 \end{bmatrix}^{\mathrm{T}}, \tag{11a}$$

$$\mathbf{T} = \begin{bmatrix} 1 & 0 & 0 & 0 \\ 0 & 1 & 0 & 0 \\ \frac{2ik(\eta_1 - \eta_2)}{\rho_2} & -\frac{i(\gamma_1 k^2 + g(\rho_1 - \rho_2))}{\rho_2 \omega} & \frac{\rho_1}{\rho_2} & 0 \\ 0 & 0 & 0 & 1 \end{bmatrix}. \tag{11b}$$

By combining Eqs. (6) and (10), one can relate the components of $\mathbf{Y}$ (for region II) and $\mathbf{Z}$ (for region I),

$$Y_k = \sum_{l=1}^{2} C_{kl} Z_l + \frac{P_{z,0}^{(1)}}{\rho_2} A_{k3}^{-1}|_{z=h_1}, \tag{12}$$

where the intermediate matrix $\mathbf{C}$ is given by

$$\mathbf{C} = (\mathbf{A}^{-1}\mathbf{TB})|_{z=h_1}. \tag{13}$$

C. Surface boundary condition at $z=d$

The boundary condition at the free surface reads

$$\hat{\sigma}_{xz}^{(2)} = \eta_2(\partial_z V_x^{(2)} + ikV_z^{(2)}) = 0, \tag{14a}$$

$$\hat{\sigma}_{zz}^{(2)} = -P^{(2)} + 2\eta_2 \partial_z V_z^{(2)} = -(\gamma_2 k^2 + g\rho_2)U_z^{(2)} + P_{z,0}^{(2)}. \tag{14b}$$

With the equation of continuity Eq. (3) and the vertical surface displacement $u_z^{(2)} = \frac{i}{\omega} v_z^{(2)}|_{z=d}$, one can rewrite Eqs. (14) as

$$\mathbf{DY} = 0, \tag{15a}$$

$$\mathbf{EY} = P_{z,0}^{(2)}/\rho_2, \tag{15b}$$

where

$$\mathbf{D} = \begin{bmatrix} 2k\cosh(kd) \\ 2k\sinh(kd) \\ i(k^2+\kappa_2^2)\cosh(\kappa_2 d) \\ i(k^2+\kappa_2^2)\sinh(\kappa_2 d) \end{bmatrix}^{\mathrm{T}}, \tag{16a}$$

$$\mathbf{E} = \begin{bmatrix} \left(2\nu_2 k - \frac{i\omega}{k}\right)\sinh(kd) + \frac{i(\gamma_2 k^2 + g\rho_2)}{\rho_2\omega}\cosh(kd) \\ \left(2\nu_2 k - \frac{i\omega}{k}\right)\cosh(kd) + \frac{i(\gamma_2 k^2 + g\rho_2)}{\rho_2\omega}\sinh(kd) \\ 2i\nu_2 k\kappa_2 \sinh(\kappa_2 d) - \frac{k(\gamma_2 k^2 + g\rho_2)}{\rho_2\omega}\cosh(\kappa_2 d) \\ 2i\nu_2 k\kappa_2 \cosh(\kappa_2 d) - \frac{k(\gamma_2 k^2 + g\rho_2)}{\rho_2\omega}\sinh(\kappa_2 d) \end{bmatrix}^{\mathrm{T}}. \tag{16b}$$

Applying Eq. (12), one can easily transform the surface boundary condition Eqs. (15) into expressions in terms of $\mathbf{Z}$, i.e.,

$$\sum_{l=1}^{2} P_l Z_l = -\frac{P_{z,0}^{(1)}}{\rho_2} P_0, \tag{17a}$$

$$\sum_{l=1}^{2} Q_l Z_l = \frac{P_{z,0}^{(2)}}{\rho_2} - \frac{P_{z,0}^{(1)}}{\rho_2} Q_0, \tag{17b}$$

where $\mathbf{P}$, $\mathbf{Q}$, P_0, and Q_0 are defined by

$$P_l = \sum_{j=1}^{4} D_j C_{jl}, \quad P_0 = \sum_{j=1}^{4} D_j A_{j3}^{-1}|_{z=h_1}, \tag{18a}$$

$$Q_l = \sum_{j=1}^{4} E_j C_{jl}, \quad Q_0 = \sum_{j=1}^{4} E_j A_{j3}^{-1}|_{z=h_1}. \tag{18b}$$

D. Surface and interfacial dynamic susceptibilities

Solving the linear equations (17) for $\mathbf{Z}$ yields

$$Z_1 = \frac{(P_2 Q_0 - P_0 Q_2)(P_{z,0}^{(1)}/\rho_2) - P_2(P_{z,0}^{(2)}/\rho_2)}{P_1 Q_2 - P_2 Q_1}, \tag{19a}$$

$$Z_2 = \frac{(P_0 Q_1 - P_1 Q_0)(P_{z,0}^{(1)}/\rho_2) + P_1(P_{z,0}^{(2)}/\rho_2)}{P_1 Q_2 - P_2 Q_1}. \tag{19b}$$

Therefore together with the relation Eq. (12) we finally obtain the complete monochromatic plane-wave solutions. It then follows that the amplitudes of the vertical interfacial and surface fluctuations are

$$U_z^{(1)} = \frac{i}{\omega} V_z^{(1)}|_{z=h_1} = \frac{i}{\omega}\sum_{k=1}^{2} N_k Z_k = \frac{i}{\rho_2\omega}\frac{(P_0[\mathbf{Q},\mathbf{N}] - Q_0[\mathbf{P},\mathbf{N}])P_{z,0}^{(1)} + [\mathbf{P},\mathbf{N}]P_{z,0}^{(2)}}{[\mathbf{P},\mathbf{Q}]}, \tag{20a}$$

$$U_z^{(2)} = \frac{i}{\omega} V_z^{(2)}|_{z=d} = \frac{i}{\omega}\sum_{k=1}^{4} R_k Y_k = \frac{i}{\omega}\left(\sum_{l=1}^{2} M_l Z_l + \frac{P_{z,0}^{(1)}}{\rho_2} M_0\right) = \frac{i}{\rho_2\omega}\frac{[\mathbf{M},\mathbf{P},\mathbf{Q}]P_{z,0}^{(1)} + [\mathbf{P},\mathbf{M}]P_{z,0}^{(2)}}{[\mathbf{P},\mathbf{Q}]}, \tag{20b}$$

where $\mathbf{N}$, $\mathbf{R}$, $\mathbf{M}$, and M_0 are defined as

$$\mathbf{N} = \begin{bmatrix} -i[k\cosh(kh_1) - k\cosh(\kappa_1 h_1)] \\ -i[\kappa_1 \sinh(kh_1) - k\sinh(\kappa_1 h_1)] \end{bmatrix}^{\mathrm{T}}, \tag{21a}$$

$$\mathbf{R} = \begin{bmatrix} \cosh(kd) \\ \sinh(kd) \\ ik\cosh(\kappa_2 d) \\ ik\sinh(\kappa_2 d) \end{bmatrix}^{\mathrm{T}}, \tag{21b}$$

$$M_l = \sum_{k=1}^{4} R_k C_{kl}, \quad M_0 = \sum_{k=1}^{4} R_k A_{k3}^{-1}|_{z=h_1}. \tag{21c}$$

The bracket notations in Eqs. (20) are defined by

$$[\mathbf{P},\mathbf{Q}] = P_1 Q_2 - P_2 Q_1, \tag{22a}$$

$$[\mathbf{M},\mathbf{P},\mathbf{Q}] = \sum_{i,j,k=0}^{2} \epsilon_{ijk} M_i P_j Q_k, \tag{22b}$$

where ϵ_{ijk} is the Levi-Cività symbol. It is noted that each of the interfacial and surface fluctuations is affected by both of the external pressure fields. Rewriting Eqs. (20) as $U_z^{(i)} = \Sigma_j \chi_{zz}^{(ij)} P_{z,0}^{(j)}$, one therefore applies the linear response theory and obtains the self- and cross dynamic susceptibilities for the interface and the free surface

$$\boldsymbol{\chi}_{zz} = \frac{i}{\rho_2\omega[\mathbf{P},\mathbf{Q}]}\begin{bmatrix} P_0[\mathbf{Q},\mathbf{N}] - Q_0[\mathbf{P},\mathbf{N}] & [\mathbf{P},\mathbf{N}] \\ [\mathbf{M},\mathbf{P},\mathbf{Q}] & [\mathbf{P},\mathbf{M}] \end{bmatrix}. \tag{23}$$

Then, according to the generalized fluctuation dissipation theorem [17] for classical fluids, the imaginary part of the dynamic susceptibility determines the thermal fluctuation power spectrum

$$S_{zz}^{(ij)}(k,\omega) = \int dt \langle u_z^{(i)}(k,t) u_z^{(j)}(-k,0)\rangle e^{i\omega t} = 2k_B T \frac{\mathrm{Im}[\chi_{zz}^{(ij)}(k,\omega)]}{\omega}. \tag{24}$$

In general, the frequency-dependent part of the susceptibility of a linear and causal physical process is in the form of $1/(\omega^2 - \omega_0^2 + i\omega\Gamma)$, where ω_0 and Γ are defined as the propagation frequency and the damping rate, respectively. If Γ is small compared to ω_0, the power spectrum has a sharp peak at $\omega = \omega_0$, the peak width being $\Delta\omega_{\mathrm{FWHM}} \approx \Gamma$. More generally, for a system with multiple responses, e.g., a supported liquid bilayer film, the frequencies and damping rates can be straightforwardly resolved by looking for the poles of $\chi_{zz}^{(ij)}(k,\omega)$ in the lower half of the complex ω plane. In particular, propagating modes are usually suppressed on highly viscous polymeric liquids, and only those over-damped

modes characterized by Γ_m exist. Hence, when evaluated at imaginary frequencies, the susceptibility turns out to be completely real, and exhibits nonzero simple poles $\omega_m=-i\Gamma_m$ ($\tau_m \equiv 1/\Gamma_m$ are capillary wave relaxation time constants) which are the collection of positive solutions for $1/\chi_{zz}^{(ij)}(k, -i\Gamma)=0$. It follows that the intermediate scattering function, i.e., the Fourier transform of the surface or interfacial fluctuation spectrum in time representation, is given as the sum of the over-damped modes at these poles,

$$S_{zz}^{(ij)}(k,t) = S_{zz}^{(ij)}(k)\sum_m a_m(k)e^{-\Gamma_m(k)t}, \tag{25}$$

where $S_{zz}^{(ij)}(k)=k_BT\chi_{zz}^{(ij)}(k,0)$ is the total power of the spectrum; and a_m are the mode amplitudes,

$$a_m(k) = \frac{\text{Residue}[\chi_{zz}^{(ij)}(k,-i\Gamma_m)]}{\chi_{zz}^{(ij)}(k,0)\Gamma_m}, \tag{26}$$

with the total amplitudes $\Sigma_m a_m=1$. The mean vertical height fluctuation correlation is then obtained as

$$\langle u_z^{(i)} u_z^{(j)} \rangle = \int \frac{d^2k}{(2\pi)^2} S_{zz}^{(ij)}(k). \tag{27}$$

When $i=j$, Eq. (27) is the square of the roughness σ_i. At small q_z in a diffuse x-ray or neutron scattering experiment, the diffuse scattering cross section is simply a linear combination of $S_{zz}^{(ij)}(k)$ [18,19]. Surface and interface sensitive XPCS is particularly focused on the measurement of the time dependence of these height-height correlations, and thus provides information about the surface and interfacial fluctuation dynamics.

Because the fluctuations of the surface and the interface are coupled hydrodynamically, any of the four susceptibility elements in Eq. (23) contains information about the capillary wave modes, except that the mode amplitudes differ from one component to the other. For a specific bilayer system, all the modes are not necessarily apparent in the scattering experiments. The explicit analytical expressions of the bilayer susceptibilities and over-damped relaxation time constants by $\chi_{zz}^{(22)}(k,\omega)$ are derived approximately, and agree quite well with the numerical calculations [20]. However, the following discussions on bilayer models will be mainly based on exact numerical calculations. In a more general sense, the bilayer theory discussed above can be extended straightforwardly to the surface and interfacial dynamics of multilayer films with one boundary condition and one Navier-Stokes equation for each additional layer. Also, the environment above the top layer does not have to be vacuum or air as in the present study. In cases that films are submerged in other liquids, the top surface needs to be reinterpreted as an interface with an accordingly modified boundary condition taking into account the interfacial tension, environment viscosity, and external pressures. Such a calculation has been performed for a bound membrane surrounded in an incompressible liquid [21].

In the present paper we have derived the dynamics of capillary waves using the fluctuation dissipation theorem. An alternative approach to calculating the relaxation times of capillary waves is to assume a sinusoidally modulated surface as an initial condition and a trial time-dependent solution for the surface amplitude, which is an exponential relaxation. Such a method was used, for example, by Herminghaus [22]. This approach is simpler if only the relaxation times are required, but it is not obvious how to extend it to obtain more detailed information such as relative amplitudes of relaxation modes or the dynamics in situations that are not well described by a single exponential relaxation.

III. VISCOSITY INHOMOGENEITY EFFECTS ON SINGLE-LAYER SURFACE DYNAMICS

Assuming an infinite viscosity for the bottom layer (effectively like a solid substrate), the previously discussed bilayer film simply reduces to a single-layer film. We then consider surface dynamics of a single-layer film with two different boundary conditions at the substrate: nonslippage and perfect slippage.

For a supported single-layer film with thickness d, the application of nonslip boundary condition at the substrate and free surface boundary condition to Eq. (6b) yields a single surface dynamic susceptibility given by [2]

$$\chi_{zz}(k,\omega) = \chi_{zz}(k,0)\left(1 + \frac{(\nu k^2)^2}{[\omega_s(k)]^2}\frac{N_0}{D_0}\right)^{-1}, \tag{28}$$

where $\chi_{zz}(k,0)$ is the static susceptibility,

$$\chi_{zz}(k,0) = (\gamma k^2 + g\rho)^{-1}, \tag{29}$$

$\omega_s(k)$ is the dispersion relation for free surface waves on an ideal bulk liquid with an infinite depth,

$$\omega_s(k) = [(\gamma/\rho)k^3 + gk]^{1/2}, \tag{30}$$

and N_0, D_0, ζ are defined as

$$N_0 = -4\zeta(1+\zeta^2) + \zeta[4 + (1+\zeta^2)^2]\cosh(kd)\cosh(\zeta kd) - [4\zeta^2 + (1+\zeta^2)^2]\sinh(kd)\sinh(\zeta kd), \tag{31a}$$

$$D_0 = \zeta \sinh(kd)\cosh(\zeta kd) - \sinh(\zeta kd)\cosh(kd), \tag{31b}$$

$$\zeta = \kappa/k = [1 - i\omega/(\nu k^2)]^{1/2}. \tag{31c}$$

For an ultrathin film, Eqs. (29) and (30) can be readily modified to include the van der Waals interactions with the substrate [23],

$$\chi_{zz}(k,0) = [\gamma k^2 + g\rho + A_{\text{eff}}/(2\pi d^4)]^{-1}, \tag{32a}$$

$$\omega_s(k) = \{(\gamma/\rho)k^3 + [g + A_{\text{eff}}/(2\pi d^4\rho)]k\}^{1/2}, \tag{32b}$$

where A_{eff} is the effective Hamaker constant. For a sufficiently thick film, this effect on surface dynamics is very often negligible. In the case of high viscosity, e.g., a polymer melt just above its glass transition temperature, the gravitational effect is also negligible and Eq. (28) reveals a single over-damped relaxation mode with a characteristic relaxation time of

$$\tau_{\text{nonslip}}(k) \simeq \frac{2\eta}{\gamma k}\frac{H}{F}, \tag{33}$$

where F and H are dimensionless functions of kd:

$$F = \sinh(kd)\cosh(kd) - kd, \tag{34a}$$

$$H = \cosh(kd)^2 + (kd)^2. \tag{34b}$$

Equation (33) has been applied to predict the dynamics of over-damped surface capillary waves on silicon supported PS films above the bulk glass transition temperature, and showed very good agreement with the results of XPCS experiments [5,10,24].

Now consider the perfect slip boundary condition, namely, that the z component of the velocity vanishes and there is no tangential stress. In this case we find that the surface dynamic susceptibility is

$$\chi_{zz}(k,\omega) = \chi_{zz}(k,0)\left(1 + \frac{(\nu k^2)^2}{[\omega_s(k)]^2}L_0\right)^{-1}, \tag{35}$$

where

$$L_0 = (1+\zeta^2)^2\frac{\cosh(kd)}{\sinh(kd)} - 4\zeta\frac{\cosh(\zeta kd)}{\sinh(\zeta kd)}. \tag{36}$$

The corresponding relaxation time obtained from the poles of Eq. (35) is

$$\tau_{\text{slip}}(k) \simeq \frac{2\eta}{\gamma k}\frac{\cosh(kd)\sinh(kd) + kd}{\sinh(kd)^2}. \tag{37}$$

We note that both equations (33) and (37) can be reexpressed in thickness-independent forms, because $\tau_{\text{nonslip}}(k)/d$ and $\tau_{\text{slip}}(k)/d$ are functions of kd only and directly proportional to η/γ. This means that at each temperature, the behavior of the capillary waves on films with different thickness can be scaled and collapse onto a single master curve. If $kd \gg 1$, both Eq. (33) and Eq. (37) naturally reduce to the capillary wave relaxation time for highly viscous bulk liquids with infinite depth [4,25,26]

$$\tau_{\text{bulk}}(k) \simeq \frac{2\eta}{\gamma k}. \tag{38}$$

A comparison of the over-damped capillary wave relaxations from PS films with nonslip and slip boundary conditions, as well as those from bulk PS liquid, is shown in Fig. 2. Here, film thickness $d=80$ nm; viscosity $\eta=4.4\times10^5$ Nsec/m^2, and surface tension $\gamma=31.4$ mN/m are interpolated from bulk values [27,28] of PS with molecular weight $M_w=123\,000$ g/mol at 150 °C. When the capillary wavelength is much smaller than the film depth d (or wave vector is larger than $2\pi/d$ as marked by the vertical dashed line), i.e., the elliptical motions of the liquid elements engaged in surface capillary waves are much less affected by the substrate, liquid films with either nonslip [Eq. (33)] or slip [Eq. (37)] boundary conditions behave as bulk liquids [Eq. (38)].

Now we use the bilayer model to investigate the effects of viscosity inhomogeneity on surface dynamics of supported viscous polymeric films with nonslip boundary conditions at the substrate surface. The reduction of T_g of PS films is suggested to be attributed to the existence of a thin liquidlike surface layer where segments of the polymer chains bear higher mobility than those in the bulk. Following Kawana and Jones [29], we hypothesize the existence of a high mobility surface layer of thickness $h_2=10$ nm and viscosities 10, 100, 1000 times less than the bulk value on a single-layer PS film of fixed total thickness $d=80$ nm at 150 °C (Fig. 3). Surface tension $\gamma_2=31.4$ mN/m and bulk viscosity $\eta_1=4.4\times10^5$ Nsec/m are identical to those used in Fig. 2. Since the film is composed of the same material, it is reasonable to assume a zero interfacial tension $\gamma_1=0$ mN/m. Many x-ray and neutron reflectivities from single-layer PS films did not reveal less dense layers on surfaces; thus we assume the same mass density throughout the whole film. The relaxation time constants for bilayer films (2)–(4) in Fig. 3(a) are cal-

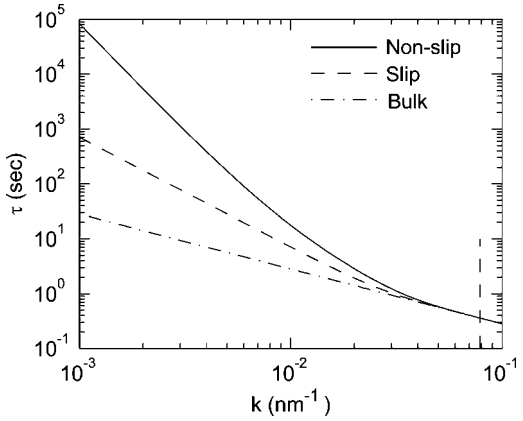

FIG. 2. Calculated relaxation time constants of the over-damped surface capillary waves on a viscous PS single-layer film with nonslip (solid), slip (dashed) boundary conditions, and on a bulk PS liquid (dashed-dotted). Wave vector at the vertical dashed line corresponds to $2\pi/d$.

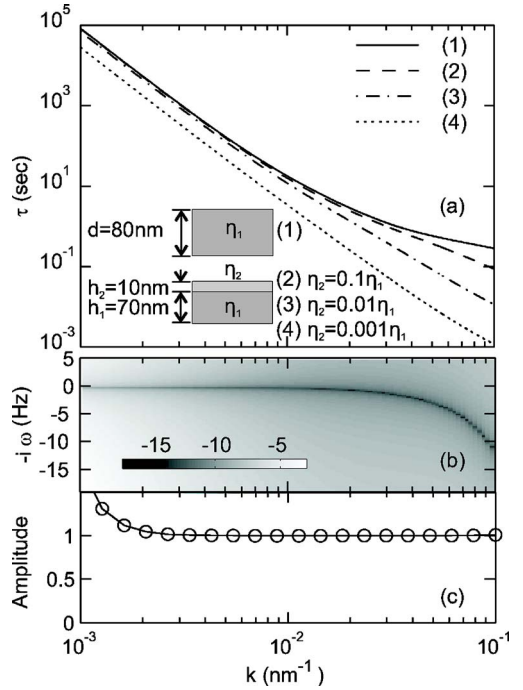

FIG. 3. (Color online) (a) Calculated relaxation time constants of the over-damped capillary waves for various supported PS films (1)–(4) at 150 °C. (b) and (c) are a logarithmic intensity map of $1/|\chi_{zz}^{(22)}(k,\omega)|$ and corresponding mode amplitude for film (2).

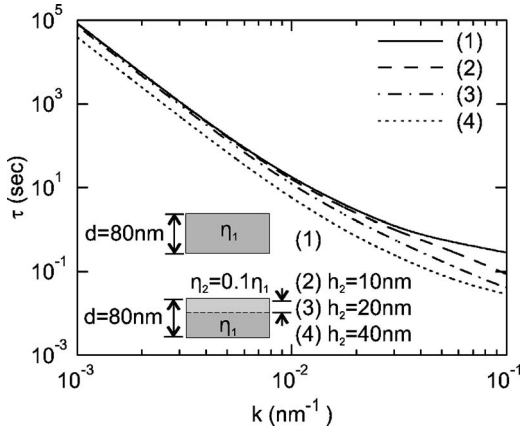

FIG. 4. Calculated relaxation time constants of the over-damped surface capillary waves from various supported PS films (1)–(4) with the same total thickness d at 150 °C. Solid line is the single-layer calculation for film (1). Other lines are bilayer calculations for films (2)–(4) whose top layer thicknesses are 10, 20, 40 nm, respectively. Other film parameters are identical to those in Fig. 3.

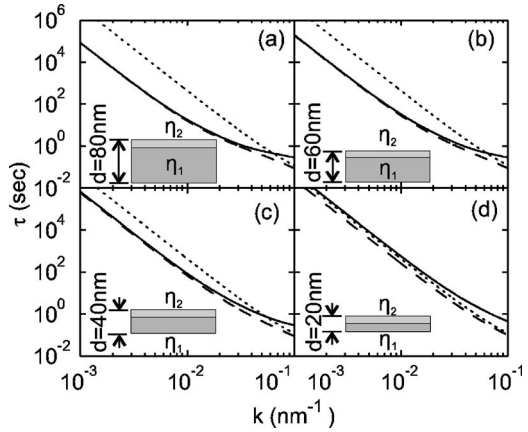

FIG. 5. Calculated relaxation time constants from various supported PS films at 150 °C. Dashed lines are bilayer calculations for films whose total thickness d is (a) 80 nm, (b) 60 nm, (c) 40 nm, and (d) 20 nm, while the thin top surface layer thickness and viscosity are fixed, $h_2=10$ nm and $\eta_2=0.1\eta_1$. Solid and dotted lines are single-layer calculations with a nonslip boundary condition for two kinds of films with parameters d and η_1 (solid lines), h_2 and η_2 (dotted lines), respectively. Viscosity of the bottom layer $\eta_1=4.4\times10^5$ Nsec/m^2 is set as the bulk value.

culated by numerically searching for purely imaginary poles of $\chi_{zz}^{(22)}(k,\omega)$ in the lower complex ω plane. A logarithmic intensity map of $1/|\chi_{zz}^{(22)}(k,\omega)|$ for bilayer film (2) is shown in Fig. 3(b), where the dark line corresponds to the solutions of $1/\chi_{zz}^{(22)}(k,-i\Gamma)=0$. The mode amplitudes of the relaxation time constants of bilayer film (2) are almost 1 and are shown in Fig. 3(c). If a nonzero interfacial tension is considered, another mode is supposed to exist. However, such a mode vanishes and does not contribute to the surface dynamics, because the PS system in the present study has zero interfacial tension. For the observed mode, the amplitude deviations at low wave vectors are attributed to the precision limit of our numerical computations. Considering the penetration of the velocity fields for the viscous liquid elements that are engaged in elliptical motions (overall effect of these motions on the surface is capillary waves), the waves with smaller wavelengths are more sensitive to the properties of the region close to surface. Therefore, this region contributes more to the overall dynamics at large wave vectors, where large deviation from the dynamics of supported homogeneous single-layer film (solid line) is observed as shown in Fig. 3(a). On the other hand, if we fix the total film thickness d and viscosities $\eta_2=0.1\eta_1$, and vary the top layer thickness $h_2=10,20,40$ nm, the surface dynamics are shown in Fig. 4. Within a typical resolution of the XPCS experiments in a reflection geometry [5], we can rule out the possibility of the existence of a more than 10-nm-thick surface layer with a viscosity smaller than one-tenth of the bulk value.

We then fix the thin surface layer viscosity and thickness, $\eta_2=0.1\eta_1$ and $h_2=10$ nm, vary the bottom layer thickness h_1 from 70, 50, 30 to 10 nm, and compare the surface dynamics to those from supported homogenous single-layer films of viscosity η_1 and thicknesses $d=80$, 60, 40, and 20 nm, respectively (Fig. 5). As the bottom layer thickness decreases, the surface dynamics (dashed lines) become more and more deviated from those of the homogeneous single-layer films with the same total thicknesses (solid lines). However, the contribution from the thin liquidlike surface layer shows prominent effects only when the thickness of this layer is comparable to that of the bottom layer.

Now consider a bilayer film with reverse viscosities $\eta_1<\eta_2$, i.e., less viscous layer at the bottom. As shown in Fig. 6, the bilayer surface dynamics gradually changes from that of a homogeneous single-layer film with a nonslip boundary condition [Eq. (33)] to that of a homogeneous single-layer film with a perfect slip condition [Eq. (37)] at the substrate. Thus the thin layer with very small viscosity underneath simulates a slip boundary condition for the top layer and plays a role as a lubricant lamella. One hypothesis for the reduced T_g of thin films is that there is a region of lowered entanglement, and thus lowered viscosity near an interface. Based on the discussion above, a relatively lower viscosity

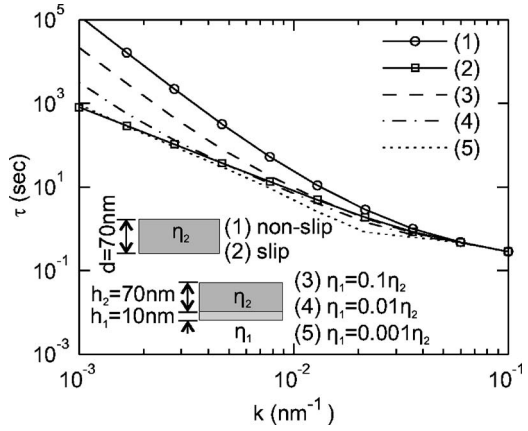

FIG. 6. Calculated relaxation time constants for samples with a homogenous viscosity [single-layer films (1), (2) with nonslip and slip boundary conditions respectively], and inhomogeneous vertical viscosity distributions [bilayer films (3)–(5) in dashed, dashed-dotted and dotted lines]. $\eta_2=4.4\times10^5$ Nsec/m^2 is the bulk value.

region near the liquid-vapor interface [film (2) in Fig. 3(a)] would have only a small effect on the capillary wave dynamics, but a region of lowered viscosity at the supported interface should significantly change the measured dynamics. The failure to see a significant deviation in the surface dynamics from that of a homogenous single-layer film by Kim *et al.* indicates that, if it exists, the region of reduced viscosity can only occur at the top surface [5]. It is interesting that recent studies of dynamics in PS/PBrS bilayer films [10] do show a modification in the dynamics consistent with a modified boundary condition at the bottom interface, and thus may indicate that the viscosity is reduced near a polymer-polymer interface, but not near a polymer-Si interface.

In a general case, for bilayer films composed of two different incompressible polymeric liquids, the interfacial tension is no longer zero and the mass densities can be different. However, our numerical calculations turn out to show that only the interfacial tension and dynamic viscosities, but not the mass densities, directly affect the dynamics, which is consistent with the approximated analytical bilayer calculations. Specifically, the capillary wave relaxations of single-layer films [Eq. (33) and (37)] do not show an explicit dependence on the mass density.

IV. VISCOELASTIC EFFECTS IN BILAYER FILMS

The discussion in the previous section considered only viscous effects, and indicated that the presence of a thin low viscous layer at the interface simulated a slip boundary condition at that interface. This has been used to interpret recent results obtained by XPCS on PS/PBrS bilayer films (see also Ref. [10]). These experiments revealed the existence of another mode arising from the interface, which basically has a wave-vector-independent relaxation time. This indicates a very large wave-vector cutoff below which the capillary waves are suppressed at the interface. This arises naturally from the current bilayer theory if we include viscoelasticity effects in terms of a complex frequency-dependent viscosity within a simple Maxwell-Debye model as discussed in Sec. II, and incorporate it into the bilayer calculations which lead to Eq. (23). We then find that all the modes obtained in the XPCS experiments [10] and the wave-vector independence of the interface relaxation time can be fitted quantitatively with reasonable values of the parameters. It has to be mentioned that the van der Waals interaction between the substrate and the film also plays a role in modulating the surface dynamics, i.e., this interaction, in a similar manner, suppresses long wavelength capillary waves below a certain van der Waals cutoff $k_{\mathrm{vdW}}=(A_{\mathrm{eff}}/2\pi\gamma)^{1/2}d^{-2}$, where A_{eff} is an effective Hamaker constant [30–32]. In a single-layer film the low wave-vector cutoff due to elasticity is simply $k_{l,c}=(3\mu/\gamma)^{1/4}d^{-3/4}$ [33,34]. Hence in a polymeric film, where $\mu > A_{\mathrm{eff}}^2/12\pi^2\gamma d^5$ holds, such suppression is usually dominated by the viscoelastic effect. Take a silicon supported PS film as an example. Given film thickness 80 nm and surface tension 31.4 mN/m, a typical value $A_{\mathrm{eff}}=5.9\times10^{-20}$ J [30,31] yields an easily fulfilled criterion $\mu > 3\times10^{-4}$ N/m^2 for PS [35].

V. SUMMARY

By applying the fluctuation dissipation theorem and linear response theory, we have calculated the surface and interfacial dynamics of liquid bilayer systems due to thermal fluctuations, which can be compared with the results of DLS or XPCS experiments. With the bilayer model, we have investigated the effect of viscosity inhomogeneities on surface dynamics, e.g., the effect of a thin layer of low viscosity either at the free surface or at the substrate. We have shown that the latter case resembles a slip boundary condition for a single-layer film at the substrate. We have also discussed the effect of introducing viscoelasticity of the films. Additionally, in a similar manner one can generalize the bilayer model to describe the interfacial dynamics of multilayer systems.

ACKNOWLEDGMENTS

We thank Jyotsana Lal for helpful discussions. This work was supported by NSF Grant DMR-0209542. H.K. acknowledges support from the International Cooperation Research Program of the Ministry of Science and Technology of Korea (M6-0403-00-0079) and 2003 Special Research Fund from Sogang University.

[1] J. L. Harden, H. Pleiner, and P. A. Pincus, J. Chem. Phys. **94**, 5208 (1991).
[2] J. Jäckle, J. Phys.: Condens. Matter **10**, 7121 (1998).
[3] D. Lumma, L. B. Lurio, S. G. J. Mochrie, and M. Sutton, Rev. Sci. Instrum. **71**, 3274 (2000).
[4] T. Seydel, A. Madsen, M. Tolan, G. Grübel, and W. Press, Phys. Rev. B **63**, 073409 (2001).
[5] H. Kim, A. Rühm, L. B. Lurio, J. K. Basu, J. Lal, D. Lumma, S. G. J. Mochrie, and S. K. Sinha, Phys. Rev. Lett. **90**, 068302 (2003).
[6] C. Gutt, T. Ghaderi, V. Chamard, A. Madsen, T. Seydel, M. Tolan, M. Sprung, G. Grübel, and S. K. Sinha, Phys. Rev. Lett. **91**, 076104 (2003).
[7] M. Sano, M. Kawaguchi, Y.-L. Chen, R. J. Skarlupka, T. Chang, G. Zografi, and H. Yu, Rev. Sci. Instrum. **57**, 1158 (1986), and references therein.
[8] *Light Scattering by Liquid Surfaces and Complementary Techniques*, edited by D. Langevin (Dekker, New York, 1992).
[9] X. Hu, X. Jiao, S. Narayanan, Z. Jiang, S. K. Sinha, L. B. Lurio, and J. Lal, Eur. Phys. J. E **17**, 353 (2005).
[10] X. Hu, Z. Jiang, S. Narayanan, X. Jiao, A. Sandy, S. K. Sinha, L. B. Lurio, and J. Lal, Phys. Rev. E (to be published).
[11] J. L. Keddie, R. A. L. Jones, and R. A. Cory, Europhys. Lett. **27**, 59 (1994).
[12] J. A. Forrest and R. A. L. Jones, in *Polymer Surfaces, Interfaces and Thin Films*, edited by A. Karim and S. Kumar

(World Scientific, Singapore, 2000).
[13] R. D. Priestley, C. J. Ellison, L. J. Broadbelt, and J. M. Torkelson, Science **309**, 456 (2005).
[14] G. B. DeMaggio, W. E. Frieze, D. W. Gidley, M. Zhu, H. A. Hristov, and A. F. Yee, Phys. Rev. Lett. **78**, 1524 (1997).
[15] J. A. Forrest, K. Dalnoki-Veress, and J. R. Dutcher, Phys. Rev. E **56**, 5705 (1997).
[16] A. M. Mayes, Macromolecules **27**, 3114 (1994).
[17] R. Kubo, Rep. Prog. Phys. **29**, 255 (1966).
[18] V. Holy and T. Baumbach, Phys. Rev. B **49**, 10668 (1994).
[19] S. Dietrich and A. Haase, Phys. Rep. **260**, 1 (1995).
[20] For more information of the analytical expressions, please visit http://sinhagroup.ucsd.edu/bilayer/supplement.html
[21] U. Seifert, Phys. Rev. E **49**, 3124 (1994).
[22] S. Herminghaus, Eur. Phys. J. E **8**, 237 (2002).
[23] M. Tolan, *X-Ray Scattering from Soft-Matter Thin Films* (Springer, Berlin, 1999).
[24] C. Li *et al.*, Macromolecules **38**, 5144 (2005).
[25] D. Byrne and J. C. Earnshaw, J. Phys. D **12**, 1133 (1979).
[26] V. G. Levich, *Physicochemical Hydrodynamics* (Prentice-Hall, Englewood Cliffs, NJ, 1962).
[27] D. J. Plazek and V. M. O'Rourke, J. Polym. Sci., Part A-2 **9**, 209 (1971).
[28] S. Wu, in *Polymer Handbook*, 4th ed., edited by J. Brandrup, E. H. Immergut, and E. A. Grulke (Wiley, New York, 1999), pp. VI-540.
[29] S. Kawana and R. A. L. Jones, Phys. Rev. E **63**, 021501 (2001).
[30] J. Israelachvili, *Intermolecular and Surface Forces*, 2nd ed. (Academic, London, 1992).
[31] I. M. Tidswell, T. A. Rabedeau, P. S. Pershan, and S. D. Kosowsky, Phys. Rev. Lett. **66**, 2108 (1991).
[32] M. Tolan, O. H. Seeck, J.-P. Schlomka, W. Press, J. Wang, S. K. Sinha, Z. Li, M. H. Rafailovich, and J. Sokolov, Phys. Rev. Lett. **81**, 2731 (1998).
[33] J. Wang, M. Tolan, O. H. Seeck, S. K. Sinha, O. Bahr, M. H. Rafailovich, and J. Sokolov, Phys. Rev. Lett. **83**, 564 (1999).
[34] Y.-S. Seo, T. Koga, J. Sokolov, M. H. Rafailovich, M. Tolan, and S. Sinha, Phys. Rev. Lett. **94**, 157802 (2005).
[35] S. Onogi, T. Masuda, and K. Kitagawa, Macromolecules **3**, 109 (1970).